Electronic Supplementary Information

Highly efficient photocatalytic reduction of CO_2 to CO using cobalt oxide-coated spherical mesoporous silicate particles as catalysts

Zi-Cheng Fu,[a] Joshua T. Moore,*[a] Fei Liang[b] and Wen-Fu Fu[b]

[a]*Department of Chemistry, Tennessee State University, 3500 John A. Merritt Blvd., Nashville, TN 37209, USA*

[b]*Technical Institute of Physics and Chemistry, Chinese Academy of Sciences, Beijing 100190, P.R. China*

Experimental section

Materials: All chemicals were of analytical grade and used as received without further purification. $Co(OAc)_2 \cdot 4H_2O$ (99%, Aladdin), $CoCl_2 \cdot 6H_2O$ (≥ 98%, Aladdin), pluronics (P123, $PEO_{20}PPO_{70}PEO_{20}$, 98%, Aldrich), cetyltrimethyl ammonium bromide (CTAB, 99%, Alfa Aesar), $NH_3 \cdot H_2O$ (Sinopharm), $[Ru(bpy)_3]Cl_2 \cdot 6H_2O$ (98%, J&K), tetraethyl orthosilicate (TEOS, 98%, Aldrich).

Catalyst characterization: X-ray diffractograms below $2\theta = 5°$ were recorded on a Bruker AXS D8 ADVANCE X-ray diffractometer. The samples with high diffraction angles were characterized by powder XRD on a Bruker AXS D8 X-ray diffractometer with Cu Kα radiation (λ = 1.54056 Å) to identify their phases. SEM images were obtained on a Hitachi S-4800 field-emission SEM. The particle size and lattice fringes of the samples were analyzed by TEM (JEM 2100 and 2100F, JEOL, Tokyo, Japan) operating at an accelerating voltage of 200 kV. The produced CO and H_2 were measured by GC (GC-2014C, Shimadzu) using Ar as the carrier gas, a 5 Å molecular sieve column (3 m × 2 mm), and thermal conductivity detector. The product of $^{13}CO_2$ isotopic experiments was analyzed with a gas mass spectrometer (Pfeiffer OmniStar). Elemental analysis of the samples was performed by ICP-AES (Varian 710-AES and Vario EL III). Specific surface areas were estimated from the amount of N_2 adsorbed at 77 K using the BET equilibrium equation. XPS was performed using a Thermo Scientific ESCALAB 250XI instrument, with an Al Kα X-ray source and power of 250 W. The C 1s binding energy was used for calibration. Raman spectroscopy was performed on a Via-Reflex confocal laser micro-Raman spectrometer with Ar^+ laser excitation (λ_{ex} = 532 nm).

Measurement of photocatalytic activity: $[Ru(bpy)_3]Cl_2 \cdot 6H_2O$ (8 mg) and CoO/s-SBA-15 or Co_3O_4/s-SBA-15 (2 mg) were dispersed in a solution of CH_3CN/TEOA/H_2O (10 mL/5 mL/5 mL) in a 60-mL quartz tube. The suspension was purged with CO_2 to remove air and then the tube was filled with CO_2 to conduct the reaction. During the photocatalytic reduction, the sealed tube containing the stirred suspension was irradiated with a 200-W white LED lamp on top of a magnetic stirrer. After the reaction, the produced gases were analyzed by GC (DINJ 50 °C, DTCD 100 °C, column temperature 50 °C, carrier gas flow 30 mL min^{-1}.

Synthesis of spherical SBA-15: CTAB (0.10 g) and KCl (1.0 g) were added to 2 M HCl (50 mL) stirred at 600 rpm and 40 °C. Ethanol (6 mL) was then added. After 20 min, P123 (2 mL) was dispersed in the solution by continuous stirring for 3 h. Then, tetraethyl orthosilicate (TEOS, 2 mL) was added dropwise to the homogeneous solution. The gel mixture was continuously stirred for another 2 h at 600 rpm and 40 °C. Thereafter, the mixture was held under static conditions at 40 °C for 24 h. The gel mixture was then transferred into a 100 mL Teflon-sealed autoclave and heated directly to 120 °C in an air-blowing thermostatic oven at a ramping rate of 3 °C min^{-1}, the temperature was maintained for 22 h. After cooling to room temperature, the resultant solid was collected by centrifugation and washed with ethanol three times. The product was dried in an oven at 60 °C. Finally, the precursor of spherical SBA-15 was calcined at 550 °C in a muffle furnace

(heating rate of 2 °C min^{-1}) in air for 6 h to remove the template.

Synthesis of spherical CoO/s-SBA-15 and Co_3O_4/s-SBA-15: The precursor of spherical SBA-15 (0.46 g) was placed in a 500-mL pear-shaped flask. Ethanol (60 mL) was added and the resulting suspension was exposed to ultrasonic treatment for 10 min at room temperature. Then an aqueous solution (1.5 mL) of $Co(OAc)_2 \cdot 4H_2O$ (0.16 g) was added dropwise to the mixture with continuous stirring at 500 rpm over 20 min. This was followed by addition of $NH_3 \cdot H_2O$ (2.2 mL). The resultant mixture was stirred at 500 rpm and 40 °C for 6 h. The solid was collected by centrifugation, washed with ethanol three times, and then dried at 60 °C in a vacuum oven. The resulting black solid powder was placed on a porcelain boat that located in the center of a horizontal quartz tube of a tube furnace. The sample was heated from room temperature to 550 °C at a rate of 2 °C min^{-1} and then held at 550 °C for 6 h under an Ar flow to produce CoO/s-SBA-15 as a light blue solid.

Co_3O_4/s-SBA-15 was synthesized by a procedure similar to that mentioned above for CoO/s-SBA-15, except that the sample was calcined at 550 °C in a muffle furnace in air to remove the template.

Synthesis of CoO nanoparticles and spherical CoO/s-SiO_2: An aqueous solution (10 mL) of $NaHCO_3$ (0.17 g) was added dropwise to 40 mL of aqueous solution containing $CoCl_2 \cdot 6H_2O$ (0.48 g) with vigorous stir in nitrogen atmosphere at room temperature. After stirring for 3 h, the resulting suspension was treated by centrifugation, washed with ultrapure water and anhydrous ethanol three times, and then dried at 60 °C in a vacuum oven. The gained white powders were distributed on a porcelain plate and transferred at the centre of a horizontal quartz tube and heated from room temperature to 450 °C at a rate of 2 °C min^{-1}, and then held at the temperature for 4 h under an Ar flow. The gray CoO nanoparticles of size distributed among 20~30 nm were formed.

The silica spheres (s-SiO_2) sized at about 100 nm were prepared according to the classical stöber method.[1] The s-SiO_2 (0.30 g) powders were dispersed in 60 mL of ethanol by ultrasonication for 20 min, then an aqueous solution (5 mL) containing $CoCl_2 \cdot 6H_2O$ (0.15 g) was slowly added to above suspension with stir at 40 °C. After stirring for 2 h, an equimolar aqueous solution (5 mL) of $NaHCO_3$ (0.05 g) was added dropwise to the reaction system, and the resultant mixture was stirred at 40 °C for 3 h. The subsequent preparation process for CoO/s-SiO_2 is similar to the procedure of CoO nanoparticles.

Computational methods: The DFT calculations were performed by the ultrasoft pseudopotentials[2] and GGA-PBEsol functional[3] using CASTEP package.[4] A 500 eV planewave basis cutoff energy was used throughout our calculations and the Monkhorst-Pack grids[5] of 4×4×1 *k*-points were used. The convergence thresholds between optimization cycles for energy change and maximum force were set as 5.0×10^{-6} eV/atom and 0.03 eV/Å, respectively. Based on the optimized reactant and product structures, the transition state (TS) searches were performed using complete LST-QST methods[6] so as to determine activation barriers of the every reaction step.

In this work, a stoichiometric CoO (100) slab of 9.03 Å × 9.03 Å ×20.26 Å (three atomic layers) with a vacuum thickness of 16 Å was constructed to model the catalytic surface, similar to CoP[7] and Ni_2P[8] surface in our previous work. In all calculations, the atoms in the bottom two layers were fixed, but the atoms in the topmost layers, as well as C, O and H atoms, were allowed to be relaxed. The geometry structure of the isolated CO_2 molecule was optimized using a supercell of 10 Å × 10 Å × 10 Å. The calculated C−O bond length and bond angle were 1.171 Å and 179.96°, which were in good agreement with the experimental values.[9]

Taking CO_2 as an example, the adsorption energy was defined as,

$$E_{ads} = E_{(CO_2 + slab)} - [E_{(CO_2)} + E_{(slab)}]$$

where the first term is the total energy of the slab with the adsorbed CO_2 molecule on the surface, the second term is the total energy of isolated CO_2 molecule, and the third term is the total energy of the bare slab of the surface (perfect or O-vacancy slab). According to the above definitions, a negative E_{ads} value corresponds to an exothermic adsorption and the more negative the E_{ads}, the stronger the adsorption effect. Notably, CO_2 molecule can only be chemically active with V-shape on O-vacancy-containing surface, so the following CO_2 reduction steps are performed on O-vacancy (100) slab.

References

1. W. Stöber, A Fink and E. Bohn, *J. Colloid Interface Sci.*, 1968, **26**, 62.
2. D. Vanderbilt, *Phys. Rev. B*, 1990, **41**, 7892.
3. J. P. Perdew, K. Burke and M. Ernzerhof, *Phys. Rev. Lett.*, 1996, **77**, 3865.
4. S. J. Clark, M. D. Segall, C. J. Pickard, P. J. Hasnip, M. J. Probert, K. Refson and M. C. Payne, *Z. Kristallogr.*, 2005, **220,** 567.
5. H. J. Monkhorst and J. D. Pack, *Phys. Rev. B*., 1976, 13, 5188.
6. T. A. Halgren and W. N. Lipscomb, *Chem. Phys. Lett*., 1977, **49**, 225.
7. Z. C. Fu, R. Xu, J. T. Moore, F. Liang, X. C. Nie, C. Mi, J. Mo, Y. Xu, Q. Q. Xu, Z. Yang, Z. S. Lin and W. F. Fu, *Chem. Eur. J.*, 2018, **24**, 4273.
8. Y. F. Zen, Z. C. Fu, F. Liang, Y. Xu, D. D. Yang, Z. Yang, X. Gan, Z. S. Lin, Y. Chen and W. F. Fu, *Asian J. Org. Chem.*, 2017, **6**, 1589.
9. H. J. Freund and M. W. Roberts, *Surf. Sci. Rep.,* 1996, **25**, 225.

Table S1 Characterization of spherical SBA-15 material and its modified samples

Materials	BET surface area (m^2/g)	Pore volume (cm^3/g)	BJH pore diameter (nm)
s-SBA-15	429.27	0.94	5.58
CoO/s-SBA-15	441.50	0.93	5.66
Co_3O_4/s-SBA-15	440.91	0.89	5.69

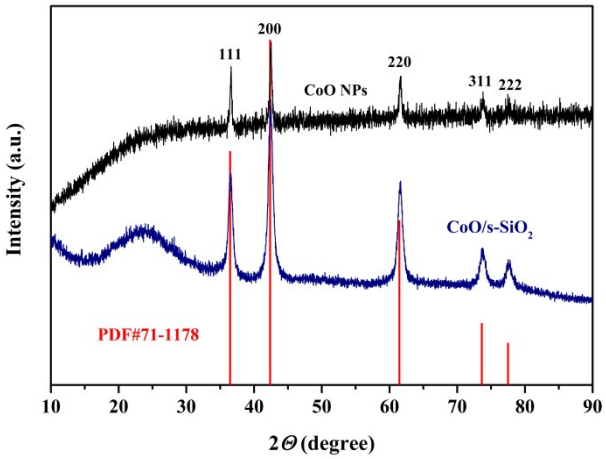

Fig. S1 XRD patterns of CoO NPs and CoO/s-SiO_2.

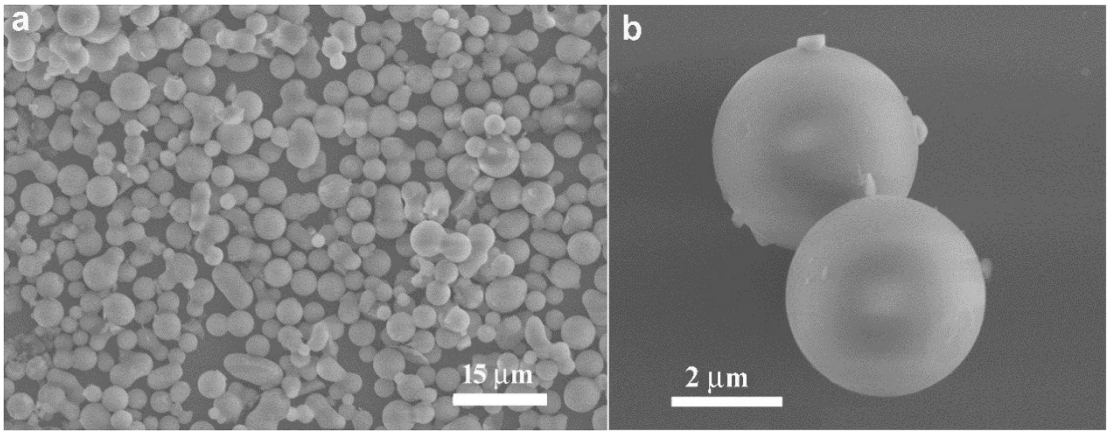

Fig. S2 SEM images of s-SBA-15 (a) and CoO/s-SBA-15 (b).

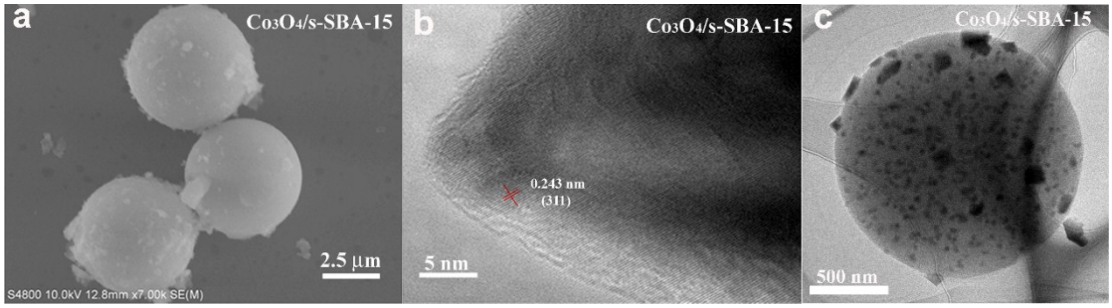

Fig. S3 (a) SEM, (b) HRTEM and (c) TEM images of Co_3O_4/s-SBA-15.

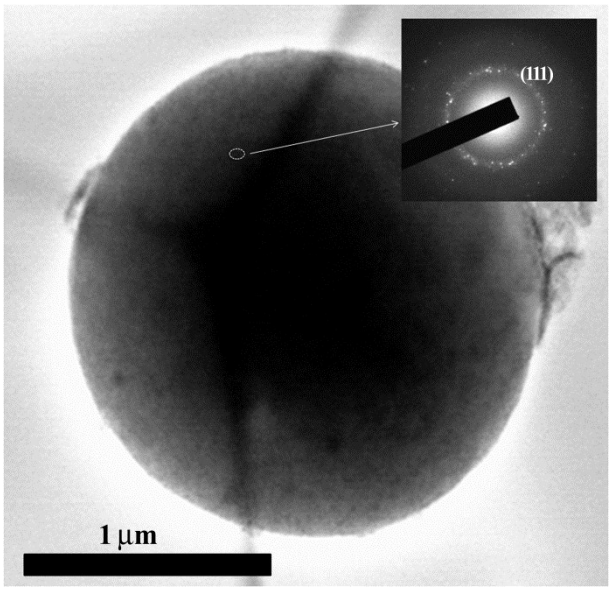

Fig. S4 TEM image and pattern (inset) of selected area electron diffraction of hybrid CoO/s-SBA-15 catalyst.

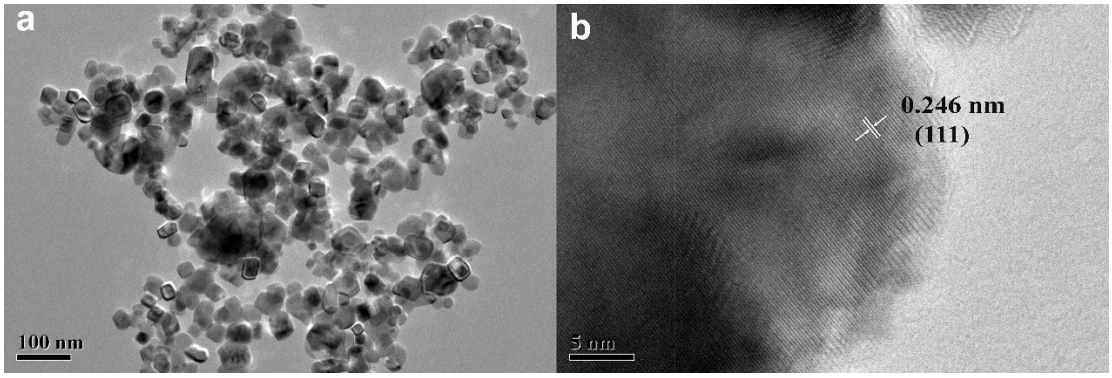

Fig. S5 (a) TEM and (b) HRTEM images of CoO NPs

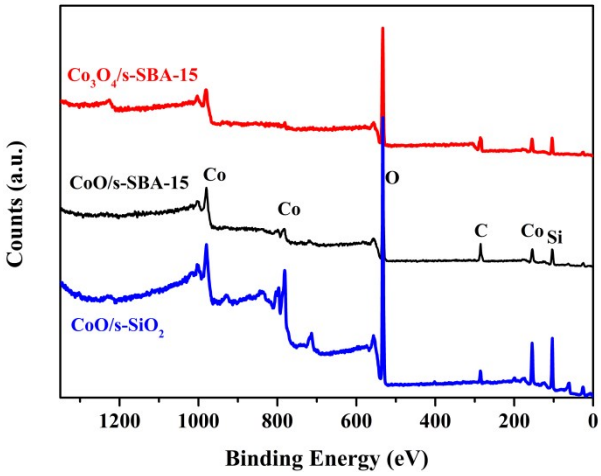

Fig. S6 XPS analysis of hybrid catalysts.

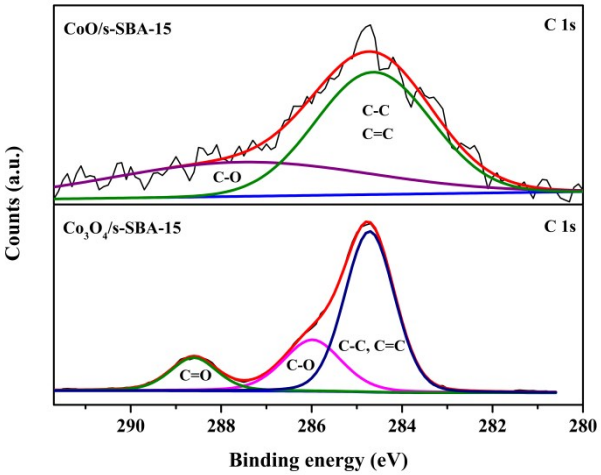

Fig. S7 High-resolution C 1s spectra of hybrids CoO/s-SBA-15 and Co_3O_4/s-SBA-15.

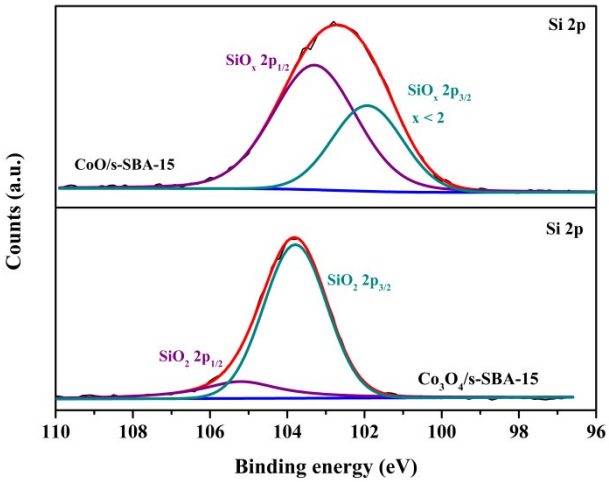

Fig. S8 High-resolution Si 2p spectra of hybrids CoO/s-SBA-15 and Co_3O_4/s-SBA-15.

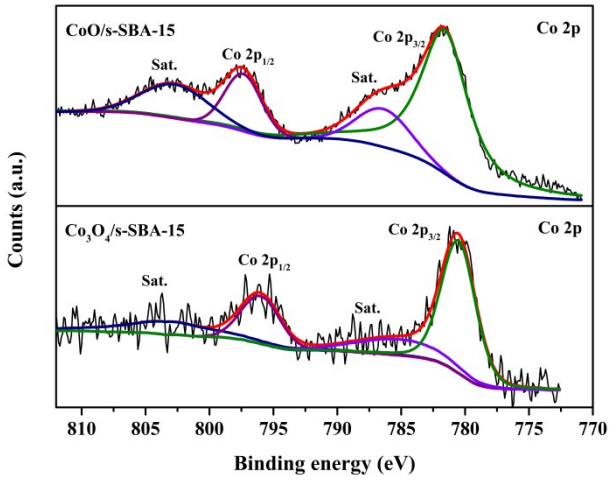

Fig. S9 High-resolution Co 2p spectra of hybrids CoO/s-SBA-15 and Co_3O_4/s-SBA-15.

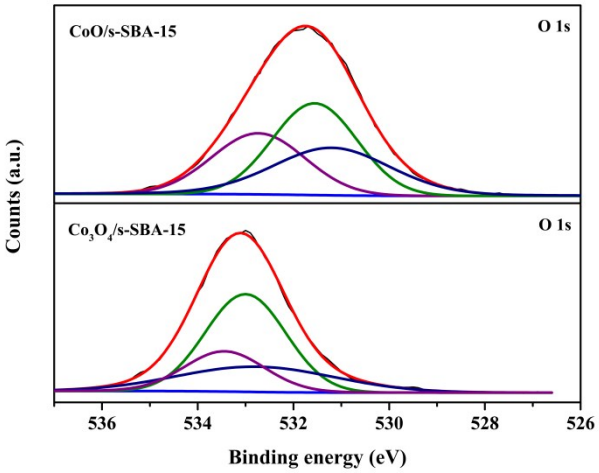

Fig. S10 High-resolution O 1s spectra of hybrids CoO/s-SBA-15 and Co_3O_4/s-SBA-15.

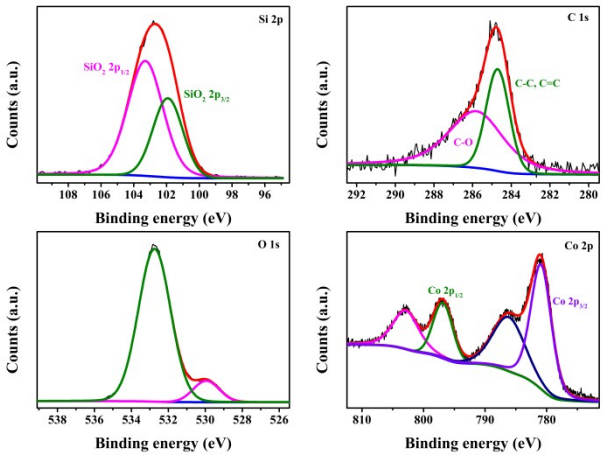

Fig. S11 High-resolution XPS spectra of CoO/s-SiO_2.

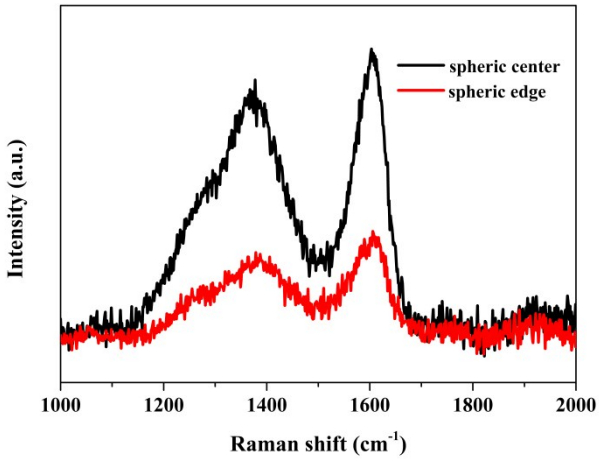

Fig. S12 Raman spectra of center and edge of hybrid CoO/s-S-SBA-15 catalyst. The peak intensity of the spherical center was remarkably higher than that of the edges, implying an increased amount of C in the macro-spherical center.

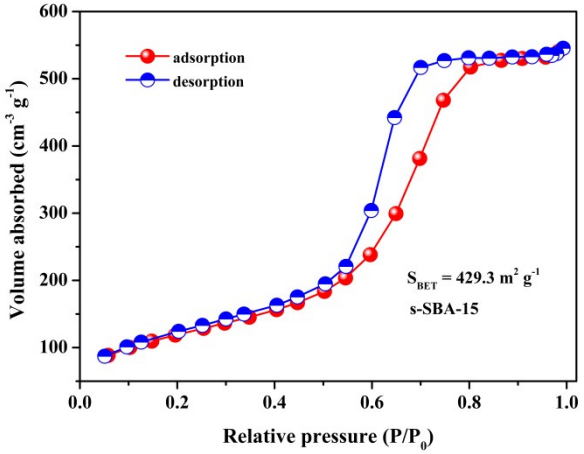

Fig. S13 N_2 adsorption–desorption isotherms of s-SBA-15.

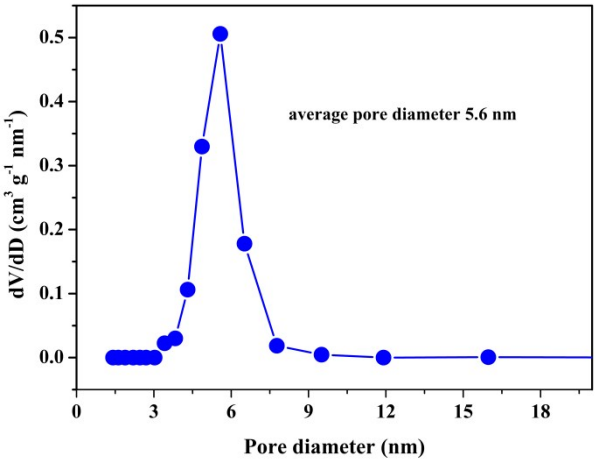

Fig. S14 Pore size distribution of s-SBA-15.

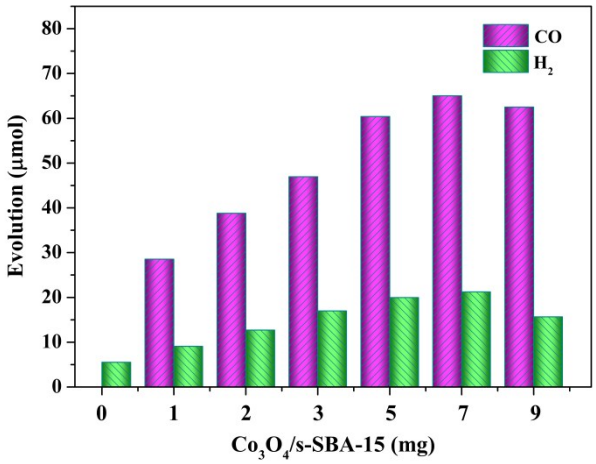

Fig. S15. Effect of Co_3O_4/s-SBA-15 content on catalytic performance in 20 mL of CO_2-saturated TEOA/CH_3CN/H_2O (v/v, 1/2/1) containing $[Ru(bpy)_3]Cl_2$ (8 mg) under irradiation of white LED lamp with stir for 2.5 h at 298 K.

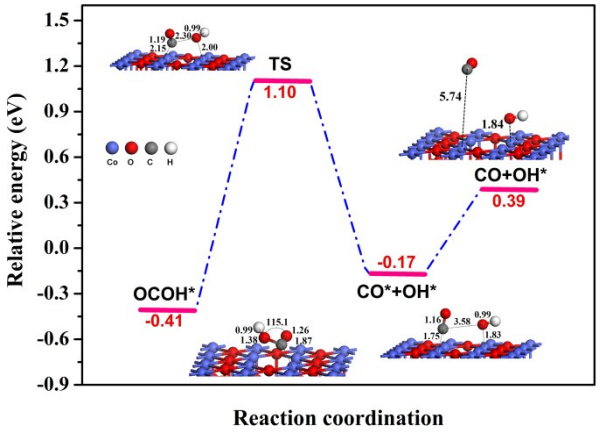

Fig. 16 Relative energy change diagram for CO_2 reduction to CO catalyzed by CoO in the presence of TEOA.

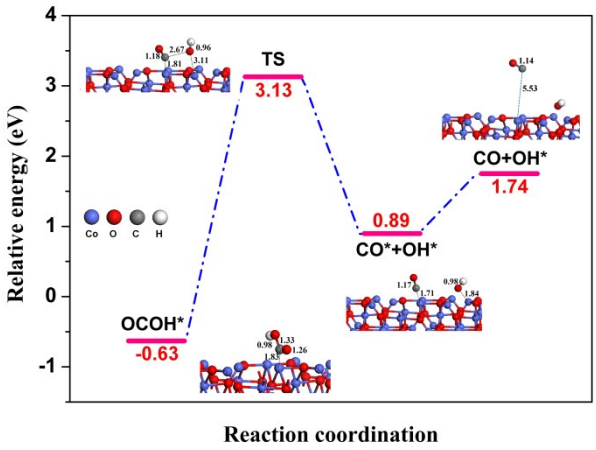

Fig. 17 Relative energy change diagram for CO_2 reduction to CO catalyzed by Co_3O_4 in the presence of TEOA.

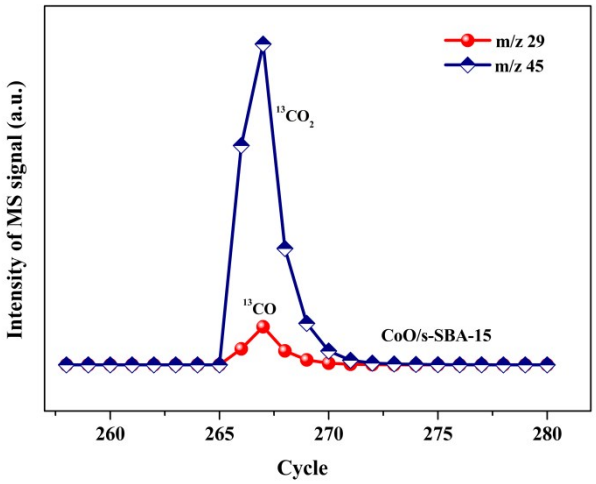

Fig. 18 MS analysis of ^{13}CO generated by photocatalytic $^{13}CO_2$ reduction.

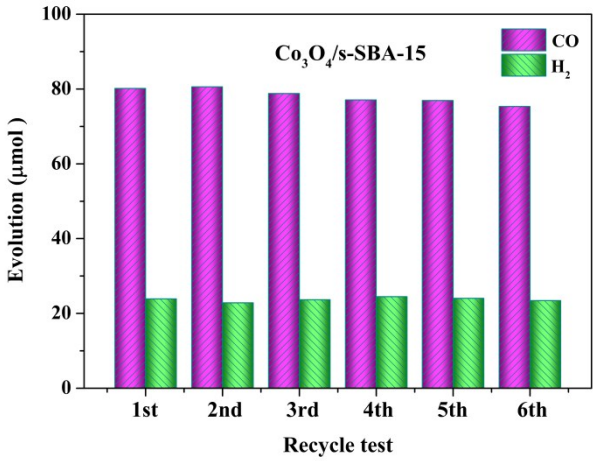

Fig. 19 Reusability of Co_3O_4/s-SBA-15 in photocatalytic CO_2 reduction.

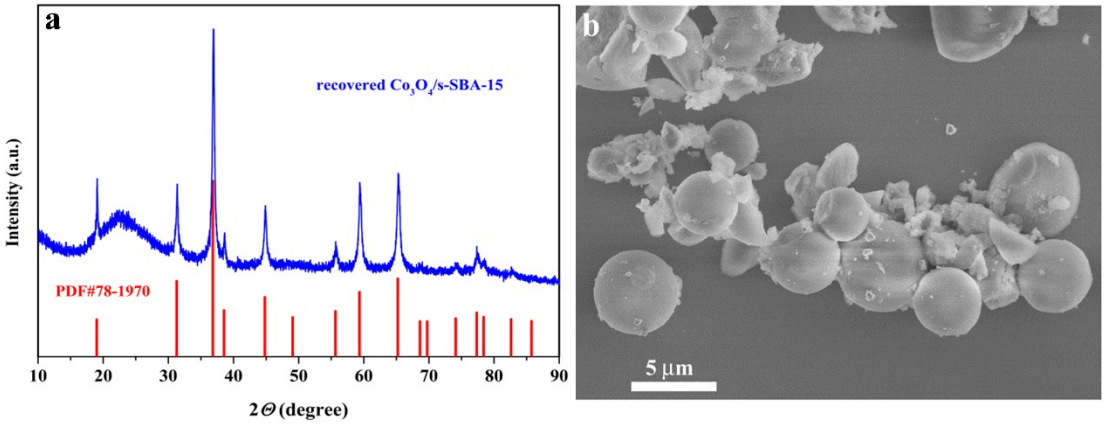

Fig. S20 XRD pattern and SEM image of used Co_3O_4/s-SBA-15.